Supplementary material

Insights into the 100 largest European surface ozone episodes during spring–summer 2003–2022

Tahimy Fuentes-Alvarez[a,*], Carlos Ordóñez[a], Ricardo García-Herrera[a,b], David Barriopedro[b], Rodrigo Crespo-Miguel[a], Miguel M. Lima[c]

[a] Departamento de Física de la Tierra y Astrofísica, Facultad de Ciencias Físicas, Universidad Complutense de Madrid, Madrid, Spain

[b] Instituto de Geociencias (IGEO), Consejo Superior de Investigaciones Científicas-Universidad Complutense de Madrid (CSIC-UCM), Madrid, Spain

[c] Instituto Dom Luiz, Faculty of Sciences, University of Lisbon, Lisbon, Portugal

* Corresponding author. E-mail address: tahifuen@ucm.es

S1. Comparison of extremes within large O_3 episodes in CAMS and observations

We have evaluated the performance of the CAMS global reanalysis in capturing local ozone extremes (local exceedances of the 95th percentile of daily O_3 maxima at each grid cell, p95) during the 100 largest episodes identified in April–September 2003–2022. For that purpose, we have compared the occurrences of local extremes in CAMS against those in an hourly gridded observational ozone dataset at 1.0° × 1.0° horizontal resolution that covers the period 2003–2015 over the domain [13° W–34° E; 36–70° N] (Schnell et al., 2014, 2015). This dataset was produced by interpolating and merging observations from the European Environment Agency's air quality database (AirBase) and the European Monitoring and Evaluation Programme (EMEP) with the objective mapping technique described in Schnell et al. (2014).

Given the limited spatiotemporal coverage of the observational dataset, only 74 out of the 100 episodes found in CAMS were used for this validation. The remaining 26 episodes from CAMS were excluded because they occurred between 2016 and 2022 (22 episodes) or covered regions that were outside the observational domain (4 episodes). Note also that a small region around the Balkans was not considered for this evaluation during 2003 due to some inhomogeneities identified in the observations (see Fig. S1 in supplement of Carro-Calvo et al., 2017).

The skill of the reanalysis in each grid cell is calculated as the number of extremes that are simultaneously found for CAMS and the observational grid, divided by the total number of extremes from CAMS in that point. Overall, a large proportion of the ozone extremes within large episodes captured by CAMS are also found in the observations. This is particularly the case over western and central Europe, with coincidences above 60% at many locations (Fig. S1). Lower coincidence rates are observed in regions with few observational sites (see Fig. S1 in supplement of Schnell et al., 2014).

Despite the overall good coincidence rates reported in Figure S1, a significant share of local extremes within large ozone episodes in CAMS do not exactly correspond to local extremes (i.e. exceedances of p95) in the observational grid. Because of this, we have carried out some additional analyses to investigate if those extremes correspond to high percentiles in the observations. For that purpose, we have proceeded as follows. For each grid cell (i,j), we first identified the days within the 74 episodes mentioned above when a local ozone extreme occurs in CAMS. We then extracted the corresponding daily O_3 maximum values from the observational dataset and stored them in a vector (V_{ij}). We finally calculated key statistics of V_{ij} (minimum, 25th, 50th, and 75th percentiles) and determined the corresponding percentile in the full observational time series (April–September 2003–2015) at that grid point. Figure S2 displays the percentile ranks in the full observational distribution that correspond to the minimum, 25th, 50th, and 75th percentiles of V_{ij} for each grid cell. The minimum observed values associated with CAMS extremes (Fig. S2a) generally lie above the 60th–70th percentiles of the climatological distribution for many grid cells of western and central Europe. Again, the lowest scores are found over the regions with low coverage of observations. Moreover, the 25th, 50th and 75th percentiles of V_{ij} typically correspond to climatological percentiles above 85th, 90th and 95th over most of Europe, respectively (Fig. S2b-d). These results confirm that, even when ozone extremes within large episodes in CAMS are not always classified as observational extremes when using the strict p95 threshold, they are consistently associated with high ozone levels in the observational record.

S2. Supplementary figures and tables

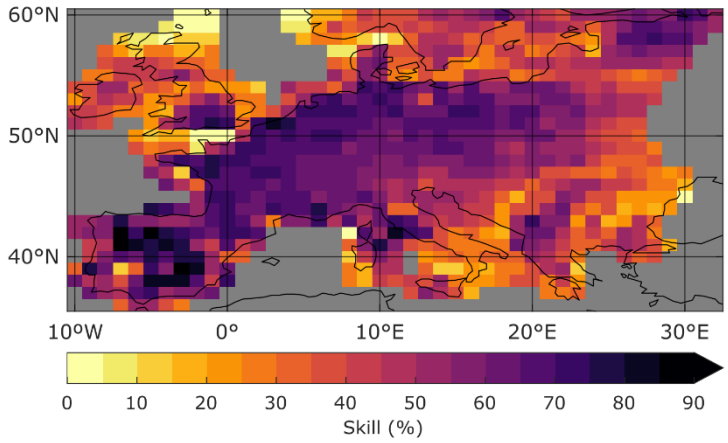

Fig S1: Skill of CAMS, defined as the percentage of local extremes (exceedances of local 95th percentiles of daily O_3 maxima) within 74 out of the 100 largest episodes identified in CAMS which are also found in the observational grid during Apil–September 2003–2015. See details in Section S1.

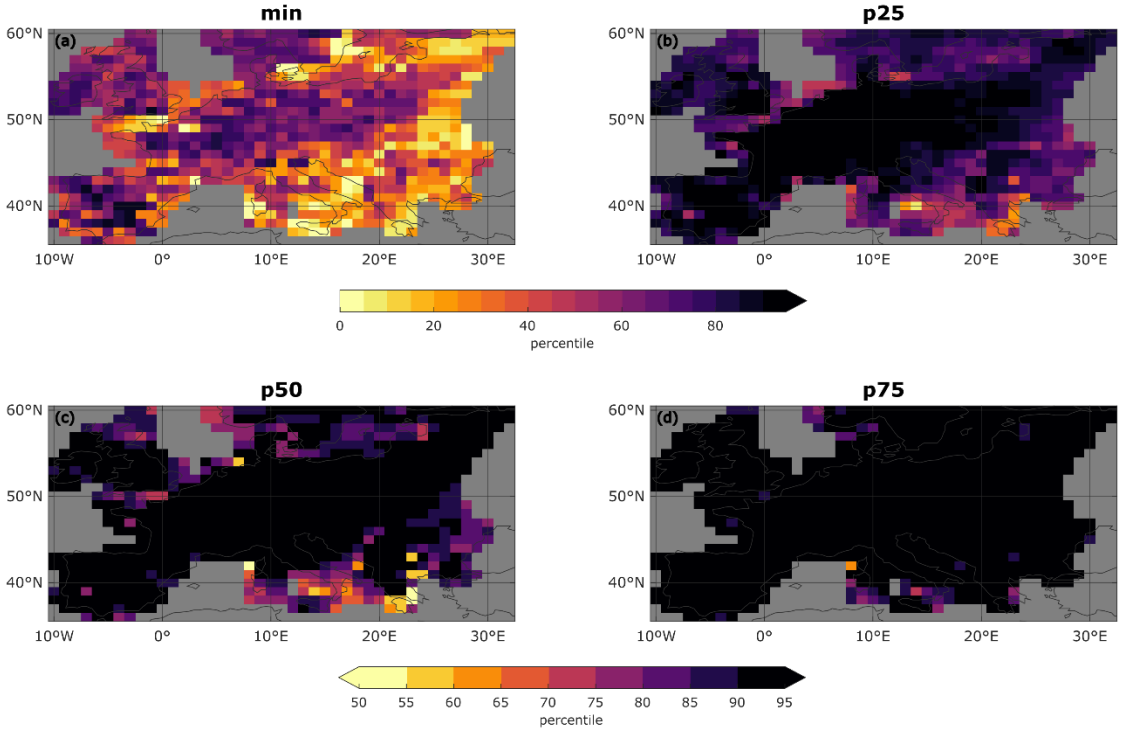

Fig S2: Percentile ranks of observed ozone during the 74 episodes evaluated for CAMS. For each grid cell, the daily maximum ozone values from the Schnell et al. (2014, 2015) observational dataset corresponding to local extremes identified within episodes in CAMS were extracted and summarised as follows: (a) minimum, (b) 25th percentile, (c) median (50th percentile), and (d) 75th percentile. Each panel shows the percentile position of these values relative to the full distribution (April–September 2003–2015) of daily ozone maxima at each grid point.

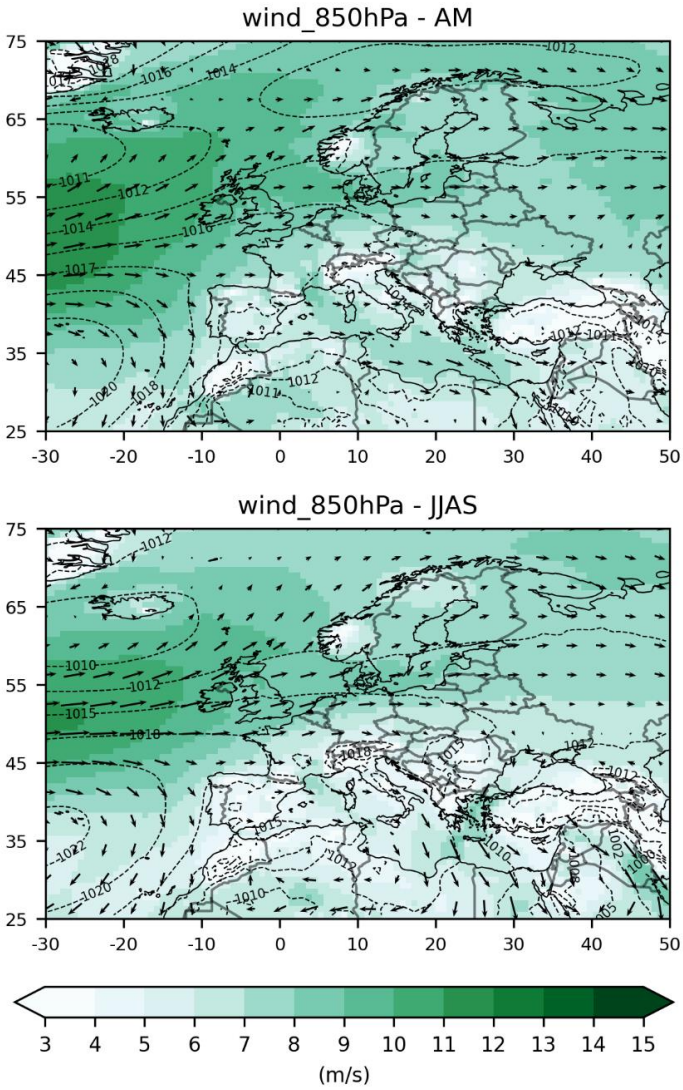

Fig. S3: Climatology of daily meteorological fields from the ERA-5 meteorological reanalysis during April–May (AM, top) and June–September (JJAS, bottom) of 2003–2022: module (green shaded, m/s) and vectors (arrows) of horizontal wind at 850 hPa as well as sea level pressure (SLP, black contour lines, hPa).

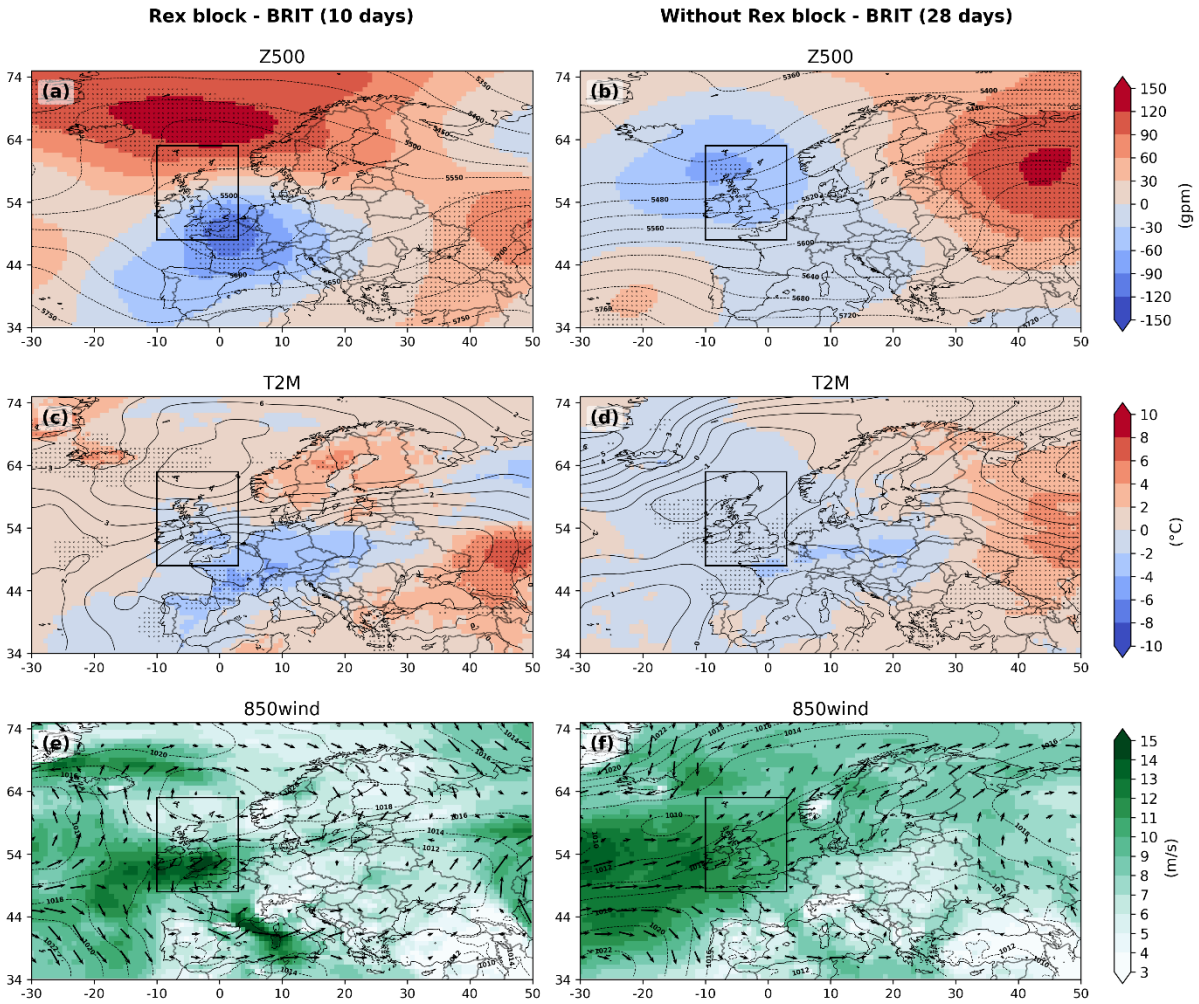

Fig. S4: Composites of daily meteorological fields from the ERA-5 meteorological reanalysis for ozone episode days in BRIT under two different regimes: (left column) days with a Rex block and (right column) days without Rex block. Panels show the (a, b) 500 hPa geopotential height anomalies (shaded, gpm) and absolute values (black contour lines, gpm), (c, d) temperature (shaded, °C) and SLP (black contour lines, hPa) anomalies and (e, f) module (green shaded, m/s) and vectors (arrows) of horizontal wind at 850 hPa as well as SLP (black contour lines, hPa).

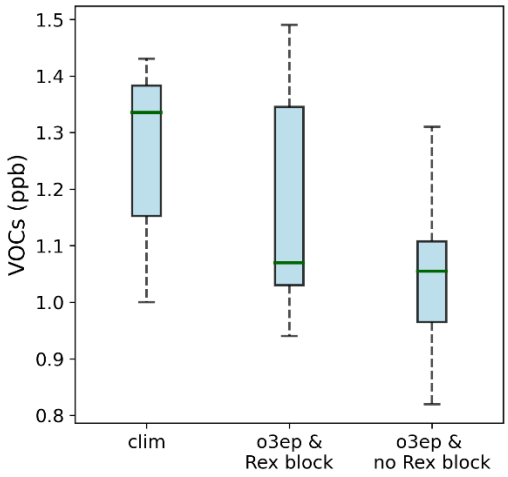

Fig. S5: Distributions of NMVOC mean concentrations (estimated as the sum of formaldehyde, ethane and propane, i.e. $[CH_2O] + [C_2H_6] + [C_3H_8]$) in BRIT. These are shown for all days during AM 2003–2022 (clim), days with ozone episode and Rex block influence (o3ep & Rex block) and with ozone episode and no Rex block influence (o3ep & no Rex block). A statistically significant difference is found only between "o3ep & no Rex block" and the climatology (p-value = 0.014) based on the two-sample Kolmogorov-Smirnov test.

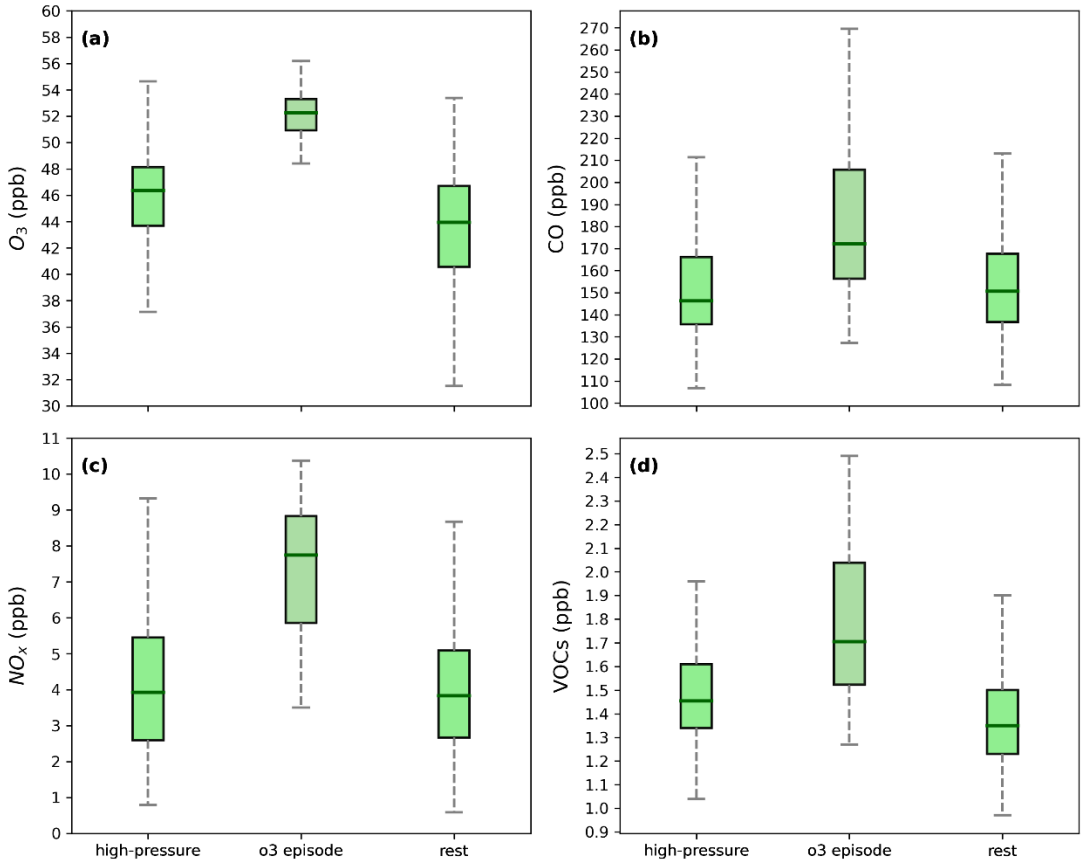

Fig. S6: Distributions of (a) daily O_3 maxima as well as daily mean (b) CO, (c) NO_x and (d) NMVOC mixing ratios (sum of CH_2O, C_2H_6 and C_3H_8) averaged over EEU during AM 2003-2022. The boxes represent the values during days with a Z500 pattern highly similar to that in Fig. 4a of the main text (high-pressure), days with ozone episode in EEU (o3 episode) and the rest of days in the analysed period (rest). The distributions on ozone episode days differ significantly from the other two distributions (p-value < 0.01 in all cases), according to the two-sample Kolmogorov-Smirnov test.

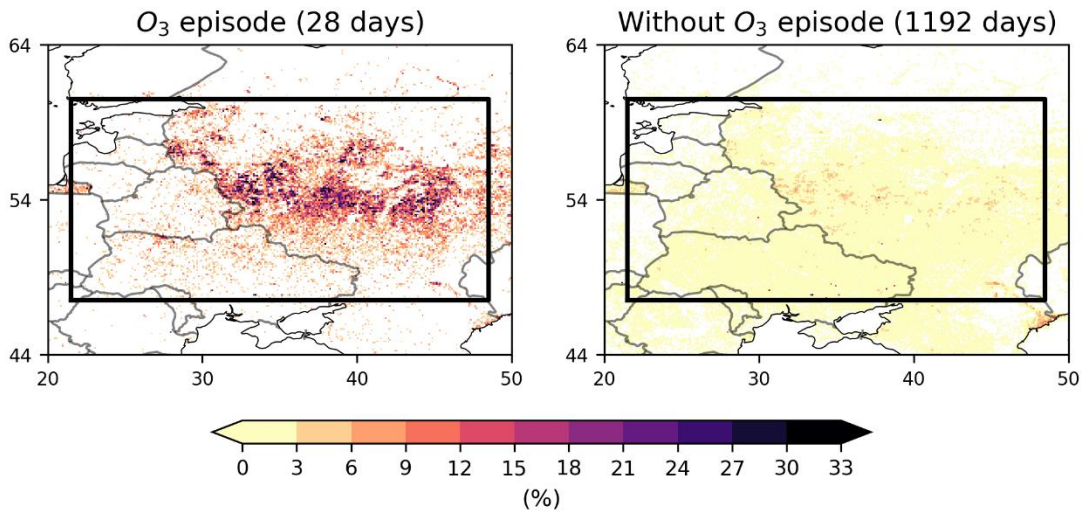

Fig. S7: Frequency of days (%) with wildfires in EEU (left) for days with ozone episodes and (right) for the rest of the days in AM 2003–2022. A 0.1° x 0.1°grid cell is considered to be affected by wildfires on a given day if the daily average wildfire radiative power from the CAMS Global Fire Assimilation System (GFAS) exceeds 0 W/m^2. The black boxes in both panels indicate the region of interest, i.e. EEU.

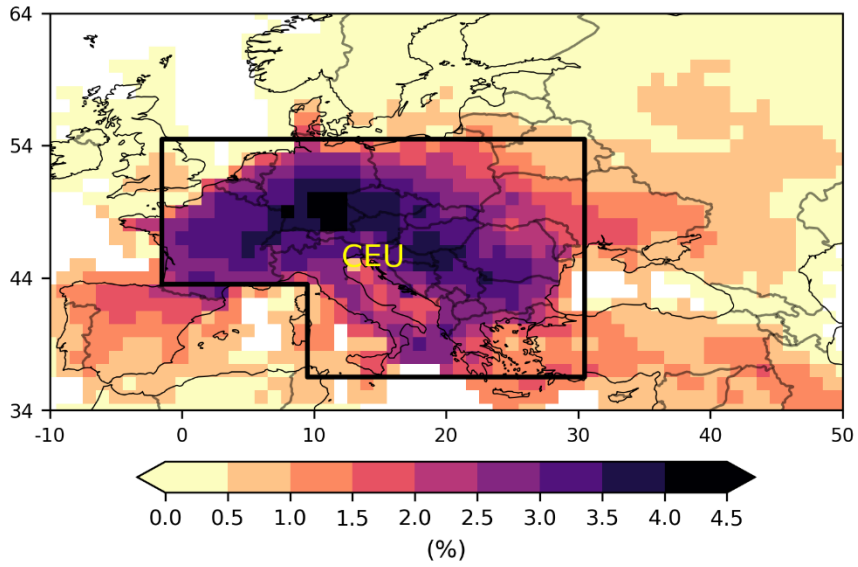

Fig. S8: As bottom panel of Figure 2 in the main text but excluding 2010.

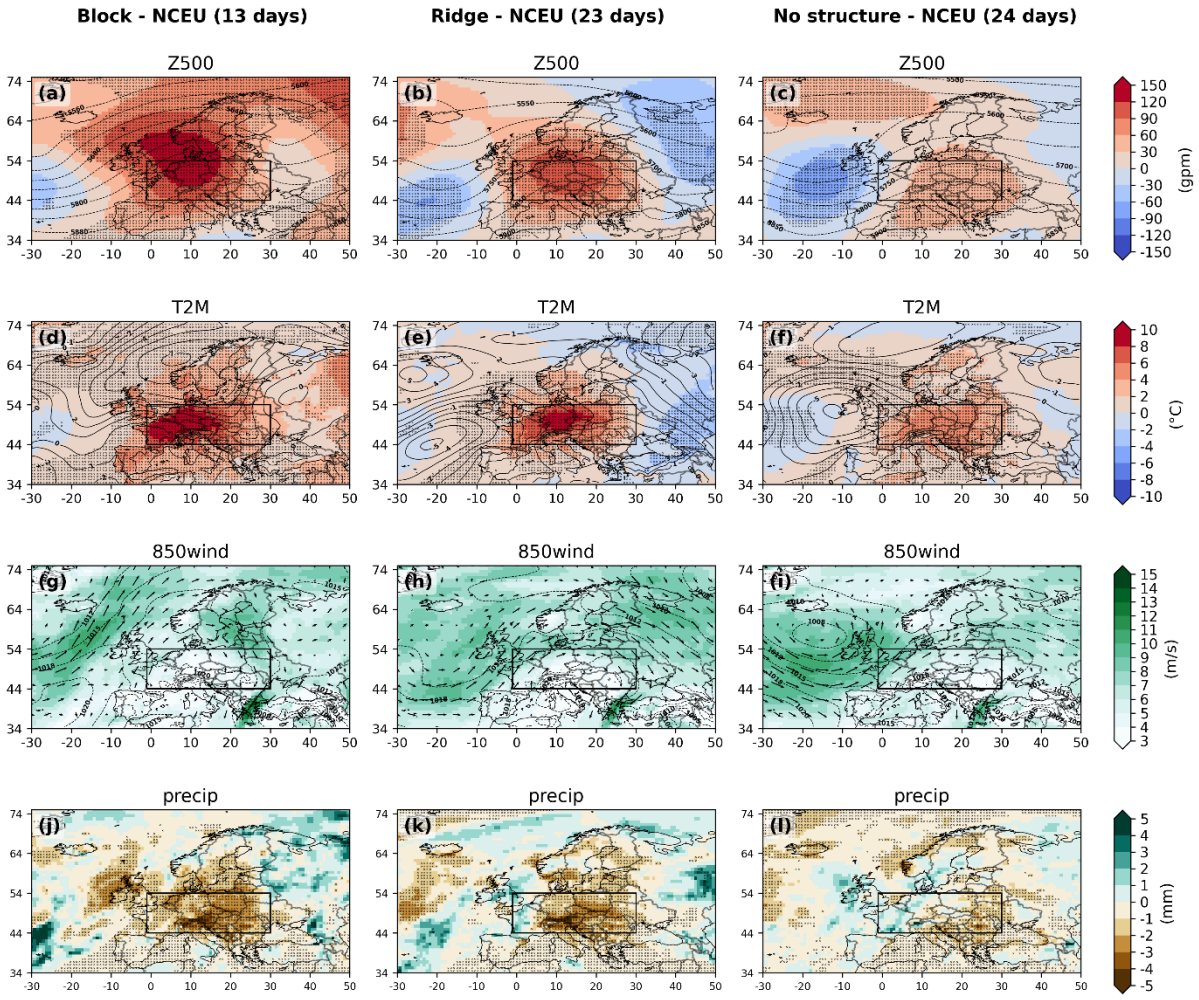

Fig. S9: Composites of daily meteorological fields from the ERA-5 reanalysis for ozone episode days (left column) with blocks, (middle column) with ridges and (right column) without block/ridge affecting NCEU: (a-c) 500 hPa geopotential height anomalies (shaded, gpm) and absolute values (black contour lines, gpm), (d-f) temperature (shaded, °C) and SLP (black contour lines, hPa) anomalies, (g-i) module (green shaded, m/s) and vectors (arrows) of horizontal wind at 850 hPa as well as SLP (black contour lines, hPa), (j-l) precipitation anomalies (mm).

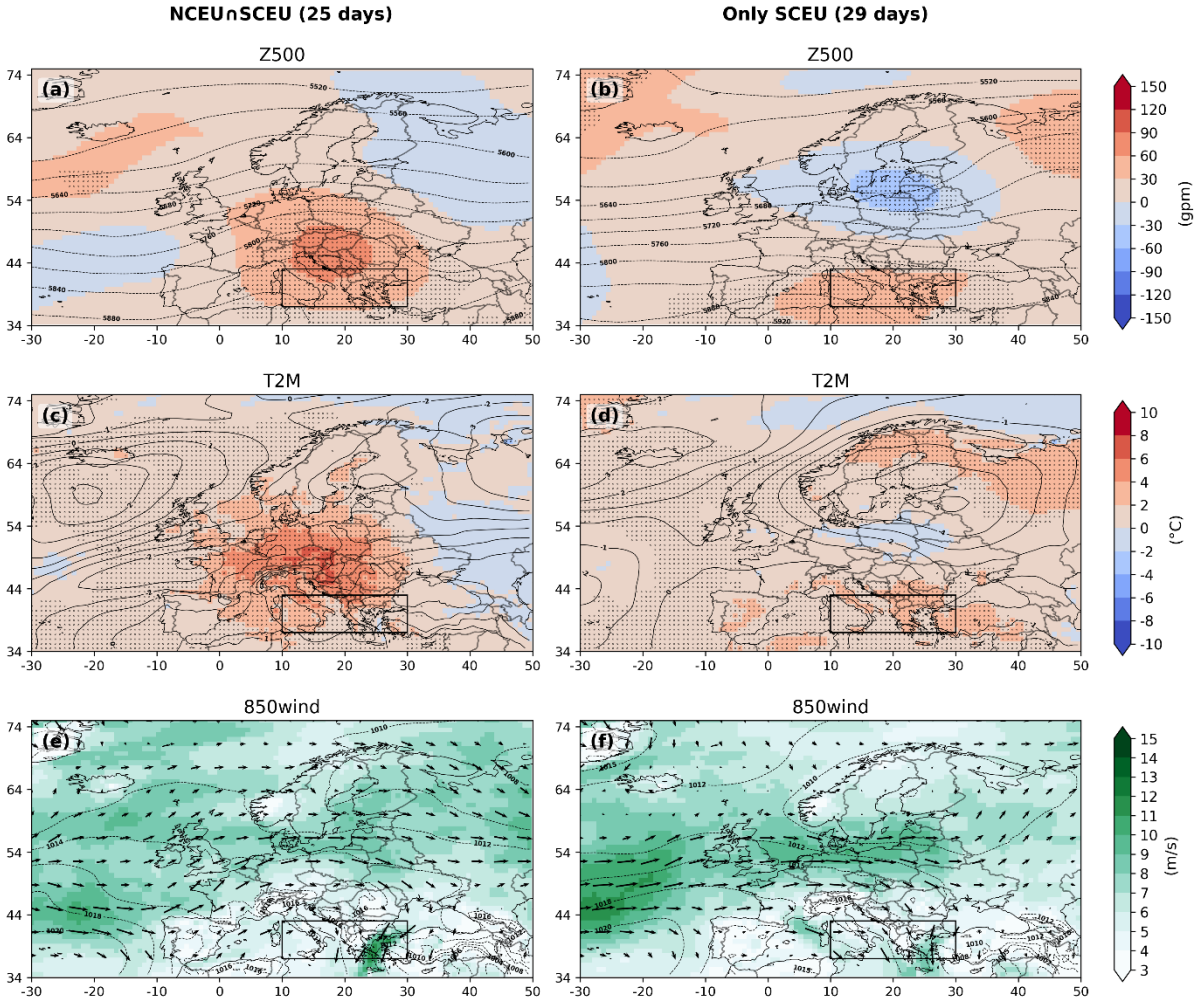

Fig. S10: As Figure S4 but for SCEU (indicated by the black rectangle) during JJAS 2003–2022. Left column for days with ozone episodes affecting both the eastern part of NCEU and SCEU (see bottom panel of Fig. 5 in main text) and right column for days with ozone episodes affecting only SCEU.

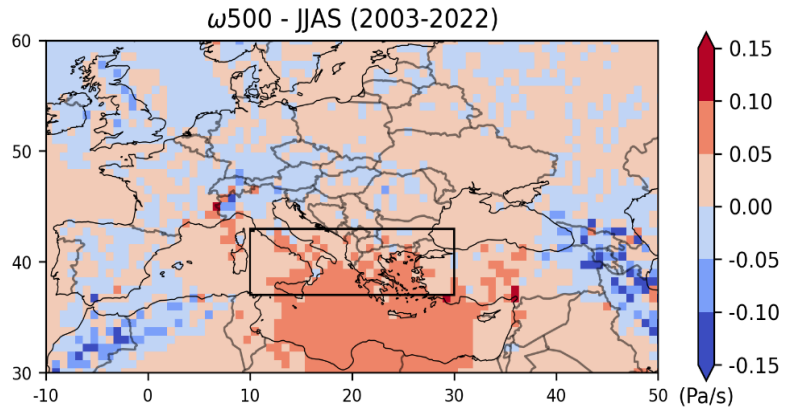

Fig. S11: Climatology of daily vertical velocity at 500 hPa (Pa/s) from the ERA-5 reanalysis averaged over all days in June–September (JJAS) of 2003–2022. Positive values represent subsidence. The box marks the location of SCEU.

Table S1: Characteristics of the main ozone episodes identified over BRIT on days without Rex block influence.

Event ID	**Dates**	**Characteristics** (*)
Event 1	01-06 Apr 2013	Easterly to northerly wind
Event 2	14-17 Apr 2013	Ridge and southwesterly wind
Event 3	13-16 May 2013	Low pressure system and westerly wind
Event 4	09-15 May 2019	Mixed circulation patterns, changing from low to high pressures; recirculation of air masses

(*) As identified from the analysis of near-surface O_3 maps over the Euro-Atlantic sector and longitudinal-vertical cross sections of O_3 within 500-1000 hPa over BRIT from the CAMS reanalysis, weather maps from the NCEP/NCAR reanalysis (https://psl.noaa.gov/data/composites/day/) and HYSPLIT backward trajectories (https://www.ready.noaa.gov/HYSPLIT.php). Last access: 09/07/2025.

References

Carro-Calvo, L., Ordóñez, C., García-Herrera, R., and Schnell, J. L. (2017). Spatial clustering and meteorological drivers of summer ozone in Europe. Atmos. Environ., 167, 496–510. https://doi.org/10.1016/j.atmosenv.2017.08.050

Schnell, J. L., Holmes, C. D., Jangam, A., and Prather, M. J. (2014). Skill in forecasting extreme ozone pollution episodes with a global atmospheric chemistry model. Atmos. Chem. Phys., 14, 7721–7739. https://doi.org/10.5194/acp-14-7721-2014

Schnell, J. L., Prather, M. J., Josse, B., Naik, V., Horowitz, L. W., Cameron-Smith, P., Bergmann, D., Zeng, G., Plummer, D. A., Sudo, K., Nagashima, T., Shindell, D. T., Faluvegi, G., and Strode, S. A. (2015). Use of North American and European air quality networks to evaluate global chemistry-climate modeling of surface ozone. Atmos. Chem. Phys., 15, 10581–10596. https://doi.org/10.5194/acp-15-10581-2015